Superconductivity and lattice instability in face-centered cubic lanthanum under high pressure

2007 J. Phys.: Condens. Matter 19 425234

(http://iopscience.iop.org/0953-8984/19/42/425234)

IOP PUBLISHING JOURNAL OF PHYSICS: CONDENSED MATTER

J. Phys.: Condens. Matter **19** (2007) 425234 (9pp) doi:10.1088/0953-8984/19/42/425234

Superconductivity and lattice instability in face-centered cubic lanthanum under high pressure

G Y Gao, Y L Niu, T Cui, L J Zhang, Y Li, Y Xie, Z He, Y M Ma[1] and G T Zou

National Lab of Superhard Materials, Jilin University, Changchun 130012, People's Republic of China

E-mail: mym@jlu.edu.cn

Received 3 August 2007
Published 18 September 2007
Online at stacks.iop.org/JPhysCM/19/425234

Abstract

The lattice dynamics and superconductivity of face-centered cubic (*fcc*) La under pressure are extensively studied using the linear-response methods within the framework of density-functional theory. A pressure-induced softening transverse acoustic (TA) phonon mode at the L point of the Brillouin zone is identified and the phonon softening pressure was predicted to be ∼4.92 GPa, which coincides with the experimentally observed second-order phase transition pressure of ∼5.3 GPa from *fcc* to distorted *fcc*. Moreover, no elastic instability is found under compression. Analysis of the calculated results suggests that the TA phonon instability is the driving force for this second-order phase transition. Furthermore, the current electron–phonon coupling (EPC) calculations suggest that the experimental observation of elevated superconducting transition temperature T_c with pressure is from the increased EPC strength and the softening TA phonon.

(Some figures in this article are in colour only in the electronic version)

1. Introduction

Lanthanum metal is the first member of the rare-earth series of elements. Like all the other rare-earth elements, La experiences a series of phase transitions under pressure. At ambient pressure, La exhibits a double-hexagonal-close-packed (*dhcp*) structure and the *dhcp* transforms to *fcc* at 2.3 GPa [1]. Low-temperature resistivity measurements [2] showed that there was a marked peak at 5.3 GPa in the residual resistance, which was attributed to the transformation from *fcc* to distorted *fcc* phase. This transition was further confirmed by the measured superconducting anomaly at ∼5.4 GPa [7]. However, the room-temperature high-pressure x-ray diffraction experiment [3] suggested that this phase transition occurred

[1] Author to whom any correspondence should be addressed.

at about 7 GPa. The temperature effects mainly contribute to the difference among the three experimental measurements. Through x-ray diffraction experiments, Grosshans *et al* speculated that a soft phonon mode at the L point of Brillouin zone (BZ) in *fcc* La might be responsible for this phase transition [3]. Wang *et al* [4] using frozen-phonon calculations also suggested that the transverse acoustic phonon at the L point softens with pressure, but no direct evidence was available in the literature. The lack of full phonon dispersion curves with pressure precludes the justification of this phonon softening at the L point.

More interestingly, different from its isoelectronic elements of Y and Sc, lanthanum is already a superconductor at ambient pressure, with a relatively high superconducting transition temperature (T_c) of 4.9 K [5]. Experimental measurements [2, 6, 7] demonstrated that T_c increases dramatically with pressure from 5 K at zero pressure to 13 K at 10 GPa. Pickett *et al* [8] calculated the electron–phonon coupling (EPC) constant λ with the rigid-muffin-tin approximation; they suggested that the drastic increase in T_c under pressure can be attributed primarily to the changes in the electronic stiffness. Wang *et al* [4] suggested that the softening of the transverse L-point phonon frequency might lead to the increased T_c; however, there are no theoretical data supporting their conclusion. In the current study, we systemically studied the lattice dynamics and the EPC with pressure using the linear-response approach based on the density-functional perturbation theory [9] to reveal the nature of the pressure-induced phase transition from *fcc* to distorted *fcc* and to uncover the physical origin for the increased T_c in *fcc* La with pressure.

2. Computational details

Pseudopotential plane-wave *ab initio* calculations were performed within the framework of density-functional theory [9]. We employ the generalized gradient approximation (GGA) for the exchange–correlation functional [11]. An ultrasoft Vanderbilt pseudopotential for La with the electronic configuration $5s^2 5p^6 5d^1 6s^2$ is used. Previous calculations of the lattice dynamics and equilibrium properties in *fcc* La have found that the effects due to the almost empty 4f bands are rather small [4]; therefore, the 4f electronic state is not included. Convergence tests gave a kinetic energy cut-off $E_{\mathrm{cut-off}}$ of 50 Ryd and a $12 \times 12 \times 12$ Monkhorst–Pack (MP) grid for the electronic Brillouin zone (BZ) integration. A $4 \times 4 \times 4$ q mesh in the first Brillouin zone was used in the interpolation of the force constants for the phonon dispersion curve calculations. The spin–orbit (SO) coupling was calculated to be negligible here, which is in good agreement with a previous theoretical calculation [8]. Note also that the effect of SO corrections is primarily to split degenerate bands along symmetry lines rather than to cause a net shift of states to higher or lower energy. Thus, it is reasonable to ignore the SO effect in this study.

The EPC spectral function $\alpha^2 F(\omega)$ could be expressed in terms of the phonon linewidth γ_{qj} due to electron–phonon scattering [18, 19]

$$\alpha^2 F(\omega) = \frac{1}{2\pi N_f} \sum_{qj} \frac{\gamma_{qj}}{\hbar \omega_{qj}} \delta(\omega - \omega_{qj}) \tag{1}$$

where N_f is the electronic DOS per atom and spin at the Fermi level ε_f. The linewidth of a phonon mode j at wavevector q, γ_{qj}, arising from electron–phonon interaction is given by

$$\gamma_{qj} = 2\pi \omega_{qj} \sum_{knm} |g^j_{kn,k+qm}|^2 \delta(\varepsilon_{kn}) \delta(\varepsilon_{k+qm}), \tag{2}$$

where the sum is over the BZ, and ε_{kn} are the energies of bands measured with respect to the Fermi level at point k. The $g^j_{kn,k+qm}$ is the electron–phonon matrix element. The EPC constant

Table 1. Calculated equilibrium lattice parameter (a_0), bulk modulus (B_0), and the pressure derivative of the bulk modulus (B_0'). Previous theoretical calculations [12] and experimental results [13, 23] are also shown for comparison. The units for a_0 and B_0 are in au and kbar, respectively.

	a_0 (au)	B_0 (kbar)	B_0'
This work	10.0984	265.9	2.66
Reference [12]	10.0231	280	—
Exp.[a]	10.0344	248 ± 7	2.8 ± 0.2
Exp.[b]	9.9905	—	—

[a] Reference [13].
[b] Reference [23].

λ can be defined as the first reciprocal moment of the spectral function $\alpha^2 F(\omega)$ [12, 13]

$$\lambda = 2 \int_0^\infty \frac{\alpha^2 F(\omega)}{\omega} \, \mathrm{d}\omega. \tag{3}$$

The superconducting transition temperature T_c has been calculated with the McMillan formula [14],

$$T_c = \frac{\omega_{\ln}}{1.2} \exp\left(-\frac{1.04\,(1+\lambda)}{\lambda - \mu^*\,(1+0.62\lambda)}\right), \tag{4}$$

where $\omega_{\ln}$ is the logarithmic average of the phonon frequency, μ^* is the Coulomb pseudopotential parameter.

A denser $20 \times 20 \times 20$ k mesh was chosen to ensure k-point sampling convergence within Gaussians of width 0.04 Ryd in the phonon linewidth calculation, which approximates the zero-width limit in this calculation. We generate 47 uniform q points in the BZ for the evaluation of the EPC constant λ. The calculations of elastic constants were performed using the CASTEP code with a $20 \times 20 \times 20$ Monkhorst–Pack k-point mesh.

3. Results and discussion

The theoretical equilibrium lattice constant is determined by fitting the total energies as a function of volume to the Murnaghan [10] equation of state. Table 1 shows the calculated values for equilibrium lattice parameters and bulk modulus, along with another theoretical calculation [12] and the experimental results [13, 23]. It is found that the current theoretical lattice constant and bulk modulus are in good agreement with those in experiments within 3%. The calculated equation of states (EOS) of *fcc* La is compared with the experimental data as shown in figure 1. The agreement between the theoretical results and the experimental data is also satisfactory. These coincidences strongly support the choice of pseudopotential and the GGA approximation for the current study. It is important to note that there is no discontinuity predicted in this EOS calculation as shown in figure 1. We also calculated the band structure of La along the high-symmetry directions. Our theoretical results agree very well with the previous theoretical calculation [8].

Figure 2(a) shows the comparison of our *ab initio* phonon dispersion curve at zero pressure along with the experimental inelastic-neutron-scattering data at $T = 295$ K [14]. There exist two sets of experimental data, measured at low and room temperatures, respectively [14]. A dip along the $[\xi\xi\xi]$ direction was found in the low-temperature phonon spectra. However, we did not reproduce this dip in the phonon calculation. Instead, our phonon dispersion curve agrees well with the experimental data measured at $T = 295$ K except for the small deviations

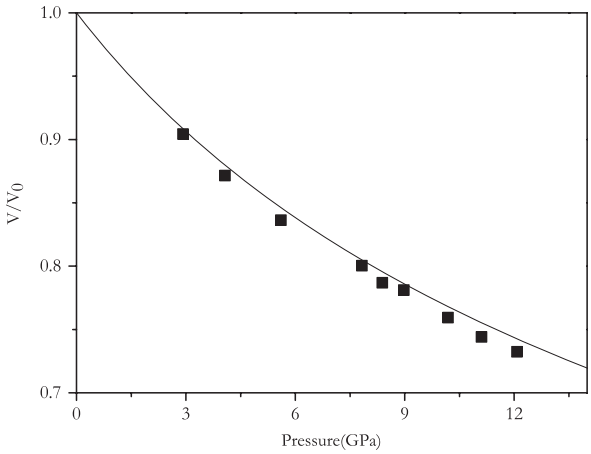

Figure 1. Comparison of the calculated equation of states (solid line) with the experimental data (symbols) [13].

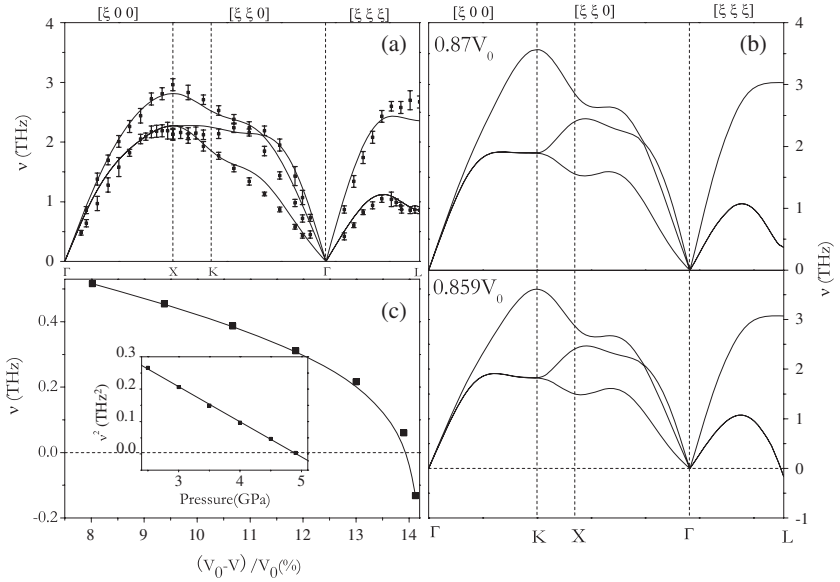

Figure 2. (a) The calculated phonon frequencies (solid lines) and phonon DOS of *fcc* La at zero pressure, together with the experimental phonon dispersion data (symbols) at $T = 295$ K [14]. (b) Calculated phonon frequencies and one-phonon DOS of *fcc* La at different volumes. (c) Main figure: calculated TA phonon frequencies at the q (0.5 0.5 0.5) point of the BZ as a function of volume. The solid line through the calculated data points represents the fitted curves using a B spline. Inset: the calculated squared phonon frequency ν^2 as a function of pressure p. The solid line through the data points is a linear fit.

of the longitudinal acoustic (LA) phonon mode near the L point and the transverse acoustic (TA) phonon branch along the [$\xi\xi$0] direction. The calculated phonon dispersion curves at different volumes are shown in figure 2(b). One can observe that with decreasing volume the TA phonon frequency at the zone boundary decreases, while other phonon modes shift to higher frequencies. At a volume of $0.859V_0$ (V_0, theoretical equilibrium volume), the TA

Table 2. Calculated and experimental [17] elastic constants of C_{11}, C_{12}, C_s and C_{44} with unit GPa for *fcc* La at ambient pressure.

	C_{11} (GPa)	C_{44} (GPa)	C_{12} (GPa)	C_s (GPa)
This work	42.8	17.8	22.4	10.2
Reference [17]	29.4	16.8	16.6	6.4
Exp.	34.5	18.0	20.4	7.1

phonon frequency at the L (0.5 0.5 0.5) point softens to imaginary frequencies, signaling a structural instability in the *fcc* phase. Figure 2(c) shows the variation of the frequency of the TA (L) mode with volume. The squared phonon frequencies ν^2 for the TA branch at the L point with pressure are also plotted, as shown in the inset of figure 2(c). A near perfect linear relation between ν^2 and p is obtained. Such a behavior is consistent with the Landau theory of pressure-induced soft-mode phase transitions [15]. The estimated transition pressure is ∼4.92 GPa ($V = 0.861V_0$), which is in good agreement with the experimental result of ∼5.3 GPa, [2] thus signifying the transition from *fcc* to distorted *fcc* phase.

To search for the structure of the distorted *fcc* phase in La based on the predicted soft mode at the zone boundary, one has to construct properly a supercell. This supercell requires the atomic vibrations to fit in a unit cell whose lattice vector of the reciprocal lattice is exactly the wavevector of the soft phonon mode. In our case of TA phonon softening at the zone boundary of the L (0.5, 0.5, 0.5) point, the doubling of the primitive cell is necessary to accommodate properly the atomic vibrations. Then one can search for the local energy minima by displacing the atom along the eigenvector direction of the mode with the largest negative eigenvalue. In many cases, one can obtain an energy well to locate the energy minimum. However, in this work, we failed to find the energy minimum because of the formation of an energy barrier instead of an energy well with the atomic displacement. This fact precludes us from predicting the distorted *fcc* structure. The failure to find the local energy minimum might be attributed to the fact that the energy gain is determined not only by the curvature of the energy surface but by high-order terms as well as the strength of coupling to strain.

Table 2 lists the calculated elastic constants of *fcc* La with the experimental data [16] and previous theoretical results [17] at ambient pressure. It is clear that there is an excellent agreement in C_{44} between the present calculated result and that of the experimental measurement. Note also that for C_{12}, C_{11} and C_s the agreement between theory and experiment is also satisfactory. Figure 3 plots the variation of elastic constant with pressure. It is observed that all the elastic constants increase with increase of pressure without showing any softening behavior. Therefore, we conclude that the elastic constants are stable within the pressures where phonon instability occurs.

The calculated EPC parameter λ and phonon frequency logarithmic average ($\omega_{\ln}$) are listed in table 3. It is clear that the calculated λ increases with pressure and the $\omega_{\ln}$ does not show any clear dependence on pressure. Figure 4 shows the comparison of the calculated T_c with available experimental data. The Coulomb pseudopotential parameter (μ^*) used here is a standard choice of 0.12. It is found that the T_c experimentally observed by Smith [6] and Balster [2] is well reproduced by the current calculation. However, our calculated T_c is significantly below the experimental data [7]. Note that the elevated T_c with pressure is mainly from the increase of λ as listed in table 3.

The calculated phonon density of states (DOS) and EPC spectral function $\alpha^2F(\omega)$ under pressure are shown in figure 5. It is found that the shape of the phonon DOS is quite similar to that of the spectral function. This behavior suggests that nearly all the phonon frequencies

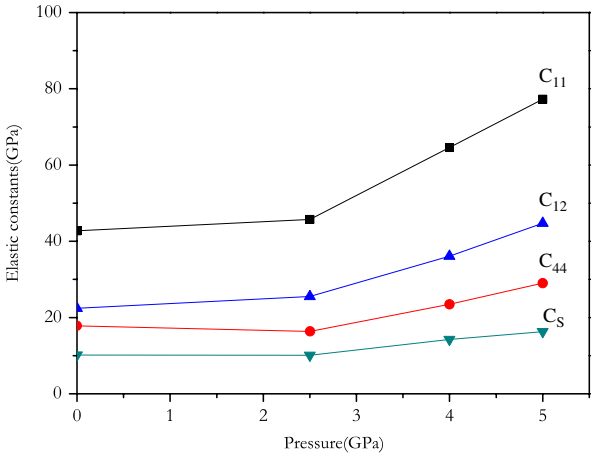

Figure 3. Calculated elastic constants (solid squares, solid up triangles, solid down triangles and solid circles) of C_{11}, C_{12}, C_s and C_{44} for *fcc* La with pressure. Solid lines are guides to the eye.

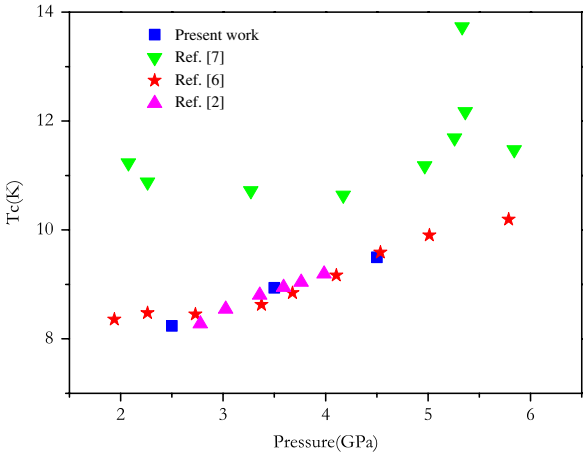

Figure 4. The superconducting transition temperature T_c as a function of pressure. Solid squares are the present results; up triangles, solid stars and solid down triangles are the experimental data [2, 6, 7].

Table 3. The calculated electron–phonon coupling constant (λ), phonon frequency logarithmic average ($\omega_{\ln}$) and electronic density of states at the Fermi level $N(E_f)$ at three pressures. The unit for $N(E_f)$ is *states/Ryd/unit cell/spin*.

Pressure (GPa)	Lambda (λ)	$\omega_{\ln}$ (cm^{-1})	$N(E_f)$
2.5	1.30	89.73	9.75
3.5	1.43	87.38	9.59
4.5	1.51	87.54	9.43

contribute to the EPC. In order to obtain more physical insights into the characteristic pressure dependence of the EPC constant λ, the calculated phonon linewidths at 2.5 GPa along several high-symmetry directions in the BZ are presented in figure 6. Except for the very small

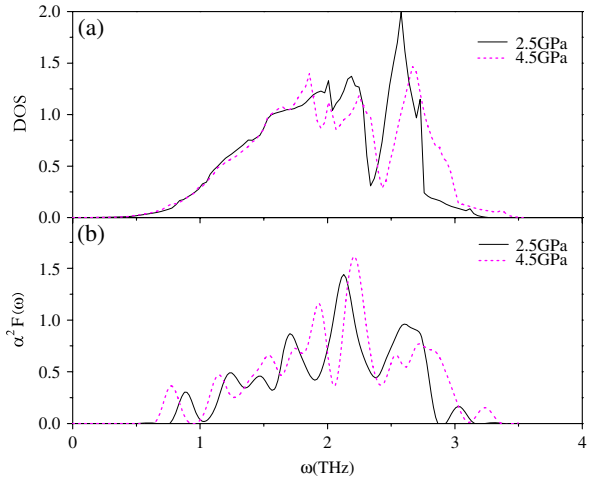

Figure 5. (a) The calculated phonon DOS at 2.5 GPa (solid line) and 4.5 GPa (dotted line), respectively. (b) The calculated spectral function $\alpha^2F(\omega)$ at 2.5 GPa (solid line) and 4.5 GPa (dotted line), respectively.

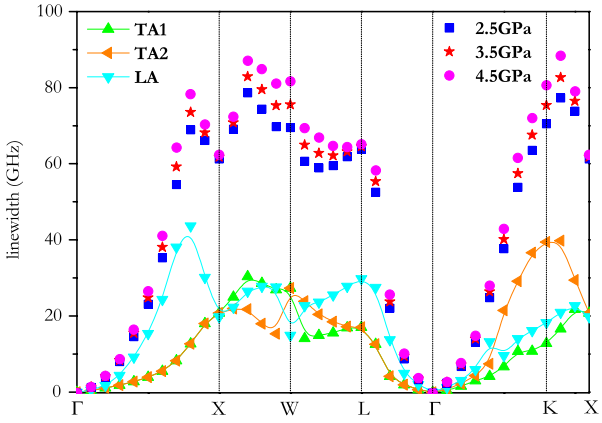

Figure 6. The calculated phonon linewidths at 2.5 GPa. The solid triangles are the calculated data for individual phonon branches. The solid lines through the data are *B* spline fits to the calculated data. The total phonon linewidths at different pressures are shown as solid squares (2.5 GPa), solid stars (3.5 GPa) and solid circles (4.5 GPa) presented along the high-symmetry directions.

and almost negligible contributions near the zone center, the phonons along other directions contribute a lot to the phonon linewidths, in agreement with the spectral function calculation. This observation indicates that the EPC in *fcc* La is isotropic, so the conventional one-band theory (i.e. averaging of coupling strengths) is sufficient to determine the transition temperature [22]. This fact also explains why the currently calculated T_c is in excellent agreement with experimental observation as depicted in figure 4. To probe the origin of the pressure-induced enhancement of λ in *fcc* La and to consider the difficulty in providing a simple description for individual phonon branches, the *total* phonon linewidths (defined as the sum of the linewidths at a given *q* point) at 2.5, 3.5 and 4.5 GPa are also compared in figure 6. It should be noted that the total phonon linewidth has no clear physical meaning and λ is related to the

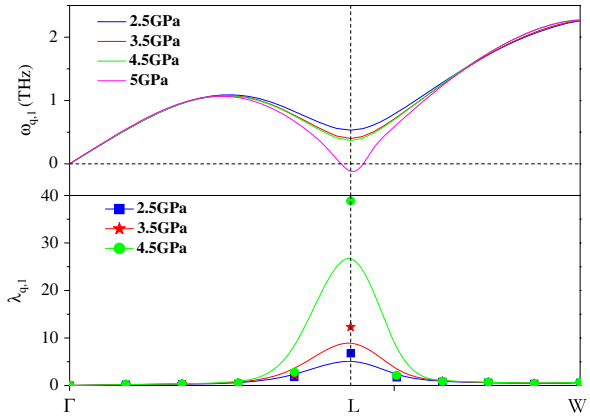

Figure 7. Upper panel: softened low-frequency transverse acoustic phonon $\omega_{q,1}$ of *fcc* La along the Γ–L–W high-symmetry line at different pressures for the TA phonon mode with lower frequency (frequencies below the zero axis denote imaginary values). Lower panel: electron–phonon coupling $\lambda_{q,1}$ calculated at different pressures. The solid lines through the data are *B* spline fits to the calculated data.

individual phonon linewidth divided by the square of the corresponding vibration frequencies; nevertheless, the calculated total phonon linewidths show a dramatic increase with increasing pressure. This behavior contributes mainly to the increased T_c with pressure.

The increased λ could be understood as follows. The EPC constant λ can be approximated by $\lambda = N(E_F)\langle I^2\rangle/(M\langle\omega^2\rangle)$ [20, 21], where $\langle I^2\rangle$ is the average square of the electron–phonon matrix element, which is related to the phonon linewidth, M is the ionic mass and $\langle\omega^2\rangle$ is the mean square of phonon frequency over the phonon spectrum. The electronic DOS at the Fermi level $N(E_F)$ under pressure is shown in table 3. Since the dominant effect of pressure on the band structure is the broadening of the bands due to the shortened atomic distance, it is reasonable to understand that $N(E_F)$ decreases with increasing pressure as listed in table 3. As shown above, the phonon linewidth increases with pressure, characterizing the increasing trend of the EPC matrix element $\langle I^2\rangle$. We argue that the softening of the low-frequency transverse acoustic phonon under pressure also contributes greatly to the increased λ. Figure 7 shows the softening low-frequency transverse acoustic phonon $\omega_{q,1}$ along the Γ–L–W direction and the corresponding q-dependence EPC $\lambda_{q,1}$ under pressure. It is obvious that the EPC $\lambda_{q,1}$ for the softened L point increases dramatically with pressure, signifying that the softening at the L point chiefly leads to the increase in EPC λ. Thus, the elevated EPC matrix element $\langle I^2\rangle$ and the softened low-frequency transverse acoustic phonon are responsible for the increased λ, in spite of the decreased $N(E_F)$.

4. Conclusion

In conclusion, the lattice dynamics and EPC of *fcc* La have been studied as a function of pressure by means of *ab initio* calculations. A soft TA phonon at the L point is verified and suggested to be the origin of the transition from *fcc* to distorted *fcc* phase. The calculated T_c is in excellent agreement with the experimental observation [2, 6]. The elevated T_c values with pressure are mainly attributable to the increased EPC matrix element $\langle I^2\rangle$ and the softening transverse acoustic phonon, in spite of an decreased electronic DOS at the Fermi level $N(E_F)$.

Acknowledgments

We thank the China 973 Program for financial support under grant No 2005CB724400, the NSAF of China under Grant No 10676011, the National Doctoral Foundation of China Education Ministry under Grant No 20050183062, the SRF for ROCS, SEM, the Program for 2005 New Century Excellent Talents in University and the 2006 Project for Scientific and Technical Development of Jilin Province. Most of the calculations in this work have been done using the Quantum-ESPRESSO [24] and CASTEP packages.

References

[1] Piermarini G J and Block S 1964 *Science* **144** 69
[2] Balster H and Wittig J 1975 *J. Low Temp. Phys.* **21** 377
[3] Grosshans W A, Vohra Y K and Holzapfel W B 1982 *Phys. Rev. Lett.* **49** 1572
[4] Wang X W, Harmon B N, Chen Y, Ho K-M and Stassis C 1985 *Phys. Rev.* B **33** 3851
[5] Finnemore D K, Johnson D L, Ostenson J E, Spedding F H and Beaudry B 1965 *J. Phys. Rev.* **137** A550
[6] Smith T F and Gardner W E 1966 *Phys. Rev.* **146** 291
[7] Tissen V G, Ponyatovskii E G, Nefedova M V, Porsch F and Holzapfel W B 1995 *Phys. Rev.* B **53** 8238
[8] Warren E P, Freeman A J and Koelling D D 1979 *Phys. Rev.* B **22** 2695
[9] Baroni S, Giannozzi P and Testa A 1987 *Phys. Rev. Lett.* **58** 1861
Giannozzi P, Gironcoli S de, Pavone P and Barone S 1991 *Phys. Rev.* B **43** 7231
[10] Murnaghan F D 1944 *Proc. Natl Acad. Sci. USA* **30** 244
[11] Perdew J P and Burke K 1996 *Int. J. Quantum Chem.* S **57** 309
Perdew J P, Burke K and Ernzerhof M 1996 *Phys. Rev. Lett.* **77** 3865
[12] McMahan A K, Skriver H L and Johansson B 1980 *Phys. Rev.* B **23** 5016
[13] Sassen K and Holzapfel W B 1975 *Solid State Commun.* **16** 533
[14] Stassis C, Smith G S, Harmon B N, Ho K-M and Chen Y 1985 *Phys. Rev.* B **31** 6298
[15] Samara G A and Peery P S 1981 *Solid State Physics* vol 36, ed H Ehrenreich, F Seitz and D Turnbull (New York: Academic)
[16] Singh N and Singh S P 1990 *Phys. Rev.* B **42** 1652
[17] Söderlind P, Eriksson O, Wills J M and Boring A M 1993 *Phys. Rev.* B **48** 9306
[18] Alen P B 1972 *Phys. Rev.* B **6** 2577
Allen P B and Silberglitt R 1974 *Phys. Rev.* B **9** 4733
[19] Schrieffer J R 1964 *Theory of Superconductivity* (New York: W A Benjamin)
[20] Hopfield J J 1969 *Phys. Rev.* **186** 443
[21] Richardson C F and Ashcroft N W 1997 *Phys. Rev. Lett.* **78** 118
[22] Pickett W 2002 *Nature* **418** 733
[23] Pearson W B 1958 *Handbook of Lattice Spacings and Structures for Metals and Alloys* (New York: Pergamon)
[24] Baroni S, Corso A Dal, Gironcoli S de and Giannozzi P, http://www.pwscf.org